

Noncollinearity of the canted spins across ultrathin Fe films on vicinal Ag surfaces

E. Jal,^{1,2} M. Dąbrowski,³ J. M. Tonnerre,^{1,2} M. Przybylski,^{3,4} S. Grenier,^{1,2} N. Jaouen,⁵ and J. Kirschner^{3,6}

¹Université Grenoble Alpes, Institut NEEL, F-38042 Grenoble, France

²CNRS, Institut NEEL, F-38042 Grenoble, France

³Max-Planck-Institut für Mikrostrukturphysik, 06120 Halle, Germany

⁴Faculty of Physics and Applied Computer Science and Academic Centre for Materials and Nanotechnology, AGH University of Science and Technology, 30-059 Kraków, Poland

⁵Synchrotron SOLEIL, Saint-Aubin, Boîte Postale 48, 91192 Gif-sur-Yvette Cedex, France

⁶Naturwissenschaftliche Fakultät II, Martin-Luther-Universität Halle-Wittenberg, 06120 Halle, Germany

(Received 6 November 2014; revised manuscript received 12 May 2015; published 12 June 2015)

We investigate the depth dependence of the canted magnetization in a bcc Fe ultrathin film grown on a vicinal Ag substrate. This study is performed for different Fe thicknesses, in the vicinity of the spin reorientation transition, by soft x-ray resonant magnetic reflectivity (SXRMR). Above 5.5 monolayers, the high spatial resolution of SXRMR allows us to describe a gradient of the canted magnetization. The tilt angle is larger near the Ag interface and decreases towards the surface. This noncollinearity is ascribed to a different balance of various anisotropies across the layer thickness. Below that value, a large increase of the tilt angle is observed and ascribed to the spin reorientation transition. Unlike the previous situation, the tilt angle is found to be homogeneous throughout the film. This can be related either to the out-of-plane spin reorientation associated to a reduced number of monolayers or to the q -space limitation of the SXRMR technique at the Fe L_3 edge.

DOI: 10.1103/PhysRevB.91.214418

PACS number(s): 75.25.-j, 61.05.cm, 75.30.Gw, 75.70.-i

I. INTRODUCTION

As part of the tremendous interest directed towards heterostructures with perpendicular magnetic anisotropy (PMA) [1], magnetic configurations exhibiting canted out-of-plane magnetization are subject to considerable attention in the field of spintronics. In magnetic data-storage media based on exchange-coupled composite layers and graded media [2], tilted magnetization brings new opportunities to improve magnetic devices as it allows for lowering the energy cost [3,4]. In spin-transfer torque devices, vertical noncollinear magnetizations are explored to reduce the switching current and time [5,6]. For spin torque oscillator applications, a spin-polarizing layer with tilted magnetization has been proposed [7], leading to the investigations of an exchange-spring magnet providing tunable magnetization tilt angle [8]. Furthermore, in PMA multilayers, canted magnetization close to interfaces allows the understanding of various magnetic properties such as magnetization reversal [9], exchange coupling between layers with in-plane (ip) and out-of-plane (oop) magnetic anisotropy [10,11], exchange bias related to a specific interfacial layer [12] or to the reorganization of the antiferromagnetic layer at the interface [13], and enhanced tunneling anisotropic magnetoresistance [14]. Finally, nonuniform oop canted magnetization arises from the competition between bulk anisotropy and surface or interface anisotropy [15–17] and has been theoretically addressed for ferromagnetic thin films [18], films grown on vicinal surfaces [19], and exchange-spring multilayers [20].

When considering the depth-resolved description, the experimental efforts on systems with tilted magnetization are scarce and challenging. Whereas magneto-optic Kerr effect (MOKE) experiments allow us to determine the thickness dependence of the tilted angle [21,22], nuclear resonant scattering [23,24], x-ray magnetic circular dichroism [25], polarized neutron reflectometry [9,26], and soft x-ray resonant magnetic reflectivity (SXRMR) [27] are used to probe the

depth dependence of the magnetization orientation. However, it remains difficult to probe the inhomogeneity of the magnetization profile at the nanometer scale [9,23,24,26]. Nonetheless, today, a fine description of the magnetization at a buried interface is highly desired for probing changes induced by currents and electric fields in perpendicular spin valves, magnetic tunnel junctions, and exchange-spring or multiferroic structures, which are potentially spatially confined close to the interface.

In this work we report on a gradient of the canted magnetization at the nanometer scale across an ultrathin bcc Fe film grown on a vicinal Ag single crystal, investigated by SXRMR. Although in most cases canted magnetization configurations are obtained by combining different layers with alternating anisotropies, the magnetization can also be canted in single layers in the vicinity of the spin-reorientation transition (SRT). In particular, for layers grown on vicinal surfaces, the canted magnetization can be detected in wide thickness range [19,22,28,29]. For thicknesses in the 5.5–10 monolayer (ML) range, the SXRMR reveals changes in the distribution of the canting angle throughout the layer with a largest oop contribution near the Ag stepped surface.

II. EXPERIMENTS

The sample is an Fe wedge of nominally 2 to 10 ML with 0.8 ML/mm slope, grown on a Ag(116) substrate and capped by 15 ML of Au in order to avoid contamination for *ex situ* measurements. Miller indexes (116) refer to vicinal surfaces with a miscut angle of 13.3°, characterized by regular (001) terraces with an average width equal to 0.86 nm, separated by monoatomic steps along the [110] direction. The details of the preparation are given elsewhere [30]. This Fe/Ag system is particularly interesting because of the oscillatory behavior of the easy axis of magnetization (EA) and of the

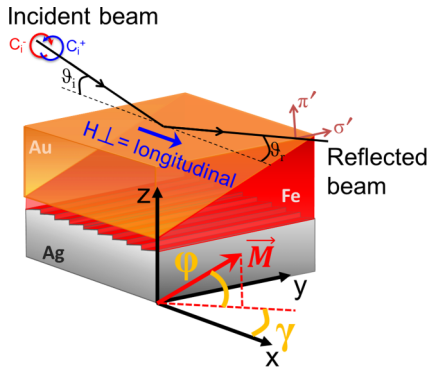


FIG. 1. (Color online) Sketch of the longitudinal configuration when the Ag steps are perpendicular to the scattering plane and definition of the angle φ (out of plane) and γ (in plane), as well as directions x , y , z in respect to the Ag steps.

oop magnetization component in the vicinity of SRT at low temperature [22,30–33].

The SXRMR experiments were performed at the RE-SOXs end station [34] on the SEXTANTS beamline [35] at synchrotron SOLEIL in France. The SXRMR is a unique probe for complex magnetic systems because of the dependence of the atomic scattering factor with respect to the incoming photon energy, scattering vector, and polarization state of the incident and reflected beam. Hence it can be used to investigate magnetic ordering and magnetic moment orientation with element and site specificity [36–39]. In this study, the measurements consist of recording two angular-dependent specular reflectivity curves, I_p and I_m , by reversing the circular polarization state of x rays with a magnetic field applied in the longitudinal direction (intersection of the scattering and surface plane, Fig. 1). This longitudinal mode allows the investigation of the ip and oop components of the magnetization [27]. To be specifically sensitive to a component of magnetization transverse to the scattering plane, a linear π polarization has been used. The data are collected with incident photon energies in the vicinity of the Fe L_3 edge (706.8 eV), allowing a sensitivity to the Fe 3d magnetic moment. The Fe wedge, which has been elaborated parallel to the Ag steps, is set transverse to the vertical scattering plane (Fig. 1). The beam size was set to 0.2×0.2 mm 2 , allowing the selection of a tranche of the wedge which leads to a distribution of nominal thicknesses limited to about 0.2 ML.

This study focuses on results obtained at low temperature (20 K) for five different Fe thicknesses. The reflected intensities are analyzed to determine the structural parameters, whereas the angular dependence of the magnetic asymmetry $(I_p - I_m)/(I_p + I_m)$ better reveals the magnetic effects related to the magnetization profile. While keeping the structural parameters fixed, the magnetic asymmetry is refined by adjusting three free parameters for each magnetic layer: a scaling factor weighting the bulk value of the bcc Fe magnetic moment ($2.2\mu_B$ [40]) and two angles φ and γ defining the orientation of the magnetic moment (Fig. 1). Specifically, φ corresponds to the canting angle of the magnetization (rotation of the magnetization in the scattering plane) and γ describes how the magnetization orientation departs from the

scattering plane in the sample plane. To meet the experimental asymmetry, the magnetic layer can be divided into several magnetic slices, allowing the derivation of a depth-resolved magnetic profile. Supplemental details of the analysis can be found in [41]. In the following analysis, the refinements focus on the changes of the φ angle. In all longitudinal cases, the γ angle has been found to be limited within 5° . These small values are assigned to a small misalignment of the steps (azimuthal rotation of the sample) with respect to the beam since the azimuthal rotation is manually adjusted.

III. RESULTS

Figure 2 shows the angular dependence of the experimental specular reflectivity curves collected at -26.8 eV below the Fe L_3 edge, i.e. at 680 eV. This allows us to strongly reduce the amplitude of the real and imaginary correction terms of the resonant atomic scattering factor, as well as to reduce the sensitivity to the magnetic terms [42]. The structural parameters are determined from the best fit (red solid line in Fig. 2) of the reflectivity data. The Fe thickness for those five positions are 6.0 ± 0.3 , 7.2 ± 0.3 , 8.4 ± 0.1 , 10.5 ± 0.3 , and 13.2 ± 0.2 Å, corresponding to about 4.2, 5, 5.9, 7.3, and 9.2 ML, respectively. The others parameters are very close within the errors bars. The Au thickness is 32.3 ± 2.1 Å except for the 5.9-ML sample from another wedge with a Au capping layer of 35.7 ± 1.5 Å. The roughnesses are of

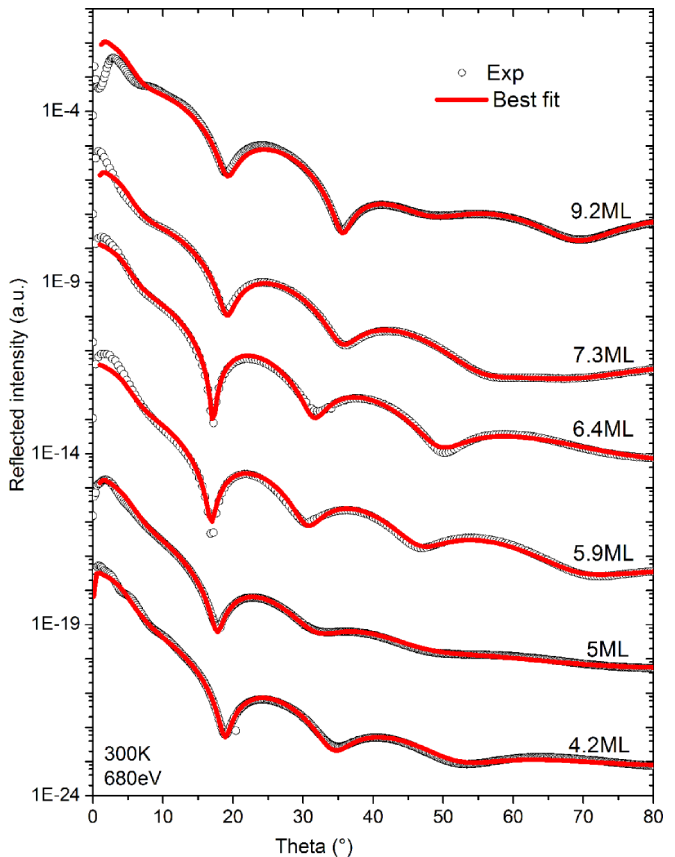


FIG. 2. (Color online) Experimental reflectivity curves (circles) and fit (red lines) for all the thicknesses at room temperature and for an x-ray energy of 680 eV and linear polarization.

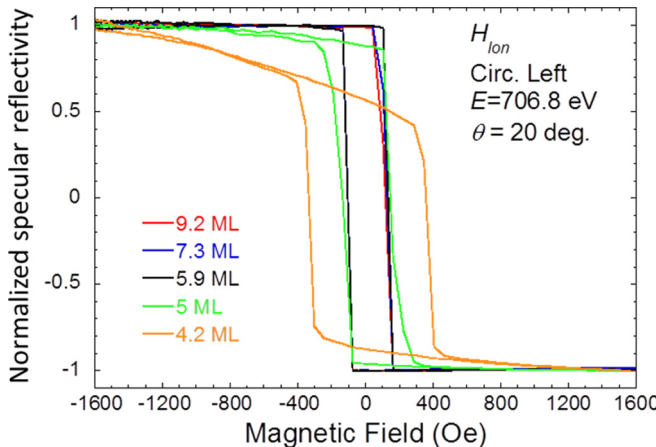


FIG. 3. (Color online) Hysteresis curves obtained at 20 K for five different thicknesses for the specular x-ray reflectivity condition with an incident angle of 20° , circular polarization, and a photon energy of 706.8 eV. The magnetic field is applied longitudinally.

$1.1 \pm 0.4 \text{ \AA}$ at the Ag interface, $1.8 \pm 0.7 \text{ \AA}$ at the Fe interface, and $3.1 \pm 0.9 \text{ \AA}$ at the Au interface. The error bars are derived from the different results obtained by refining the reflectivities for energies closer to the edge.

Figure 3 shows hysteresis loops taken for the different thicknesses. They were recorded by making use of the magnetic contrast in the specular reflectivity condition at an incident angle of 20° and a photon energy of 706.8 eV with a circularly polarized light. The field was applied along the easy axis of magnetization, which is perpendicular to the steps (i.e., along the x axis in Fig. 1). This configuration at such a low angle probes mainly the ip longitudinal component of the magnetization and is weakly sensitive to the oop component of magnetization. For thicknesses above 5.9 ML, square hysteresis loops with a coercivity of 237 Oe are measured. For 5 ML the signal at remanence decreases due to a reduced longitudinal component, whereas the switching field increases. This is directly related to the rotation of the magnetization from ip to oop due to the SRT. This effect is stronger for 4.2 ML, as illustrated by the larger reduction of the longitudinal component. The increase in the coercivity and the shape of the loop further indicate it is harder to align the magnetic moment along the applied field direction, supporting a change of the easy magnetization axis. At the maximum value of applied field, all the samples are in a single domain state.

Figure 4 presents the SXRMR results for 4.2- and 5-ML-thick layers. Figure 4(a) shows the magnetic asymmetry as a function of the specular angle θ collected at 706.6 eV for 4.2 ML under a 1600-Oe longitudinal magnetic field. The strong signal below angles of 53° is related to a net longitudinal magnetic component, whereas the signal above angles of 53° is due to the polar contribution [27]. Both components are reversed under the reversal of longitudinal magnetic field. A very good fit of the data is obtained by considering only two parameters: the amplitude of the average magnetic moment $m_{\text{Fe}} = 2.6\mu_B \pm 0.5\mu_B$ and the average tilted angle $\varphi = 26^\circ \pm 4^\circ$. The error bars are derived from the analysis performed at various energies close to the Fe L edges. This Fe magnetic moment, derived here for 4.2 ML, is in good

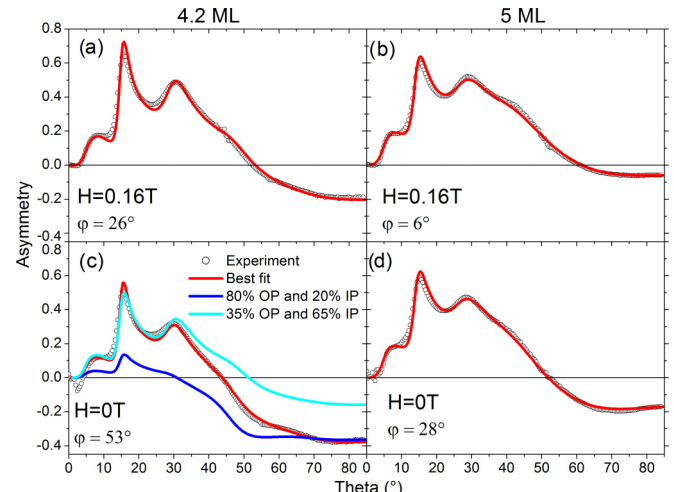


FIG. 4. (Color online) Magnetic asymmetries measured by SXRMR (circles) at 20 K using circularly polarized light and photons energy of 706.6 eV for (left) 4.2 and (right) 5 ML of Fe. (a) and (b) Results obtained by flipping a 1600 Oe longitudinal field. (c) and (d) Results obtained in a remanent state. Solid lines correspond to best fits using different free-parameter sets and calculated curves (see text).

agreement with the observation of a 20%–30% increase of the average magnetization over 2–3 ML at both Ag/Fe and Fe/Au interfaces (compared to the regular bcc Fe magnetic moment of $2.2\mu_B$ at low temperature) [41].

The magnetic asymmetry was then measured at $H = 0 \text{ Oe}$, in the remanent state, and is displayed in Fig. 4(c). We can immediately see that the amplitude is reduced at small angles and is strongly enhanced at large angles. In particular, the amplitude of the asymmetry at $\theta = 20^\circ$ is reduced by about 30%, in agreement with the change in magnetic contrast in the reflectivity observed between $H = 1600 \text{ Oe}$ and $H = 0 \text{ Oe}$ in Fig. 3. The observation of a signal at small angles shows there is still an ip component of the magnetization, and hence the magnetic configuration does not fragment into stripes of oop opposite magnetization. Indeed, this scenario would have yielded a significant reduction of the average ip component or a cancellation in the case of equivalent distribution. Moreover, the enhanced signal at large angles rules out a scenario with laterally distributed periodic domains of canted magnetization pointing up or down, which would lead to a null oop magnetic component. Therefore, the evolution of the magnetic asymmetry obtained with and without magnetic field is a direct indication of the rotation of the average magnetization towards the surface normal. The increase in the oop component occurs simultaneously with the reduction in the ip component. This rotation ends in the scattering plane since no significant net transverse magnetization can be detected by measuring the asymmetry using linear π polarization [41]. Assuming a single domain state, the fit of the data is in very good agreement with an oop rotation of the magnetization from $\varphi = 26^\circ$ to $\varphi = 53^\circ \pm 7^\circ$. However, because of the intrinsic lateral averaging of specular reflectivity, a signal with both oop and ip magnetic components might indicate either the coexistence of domains that are purely oop and ip, smaller

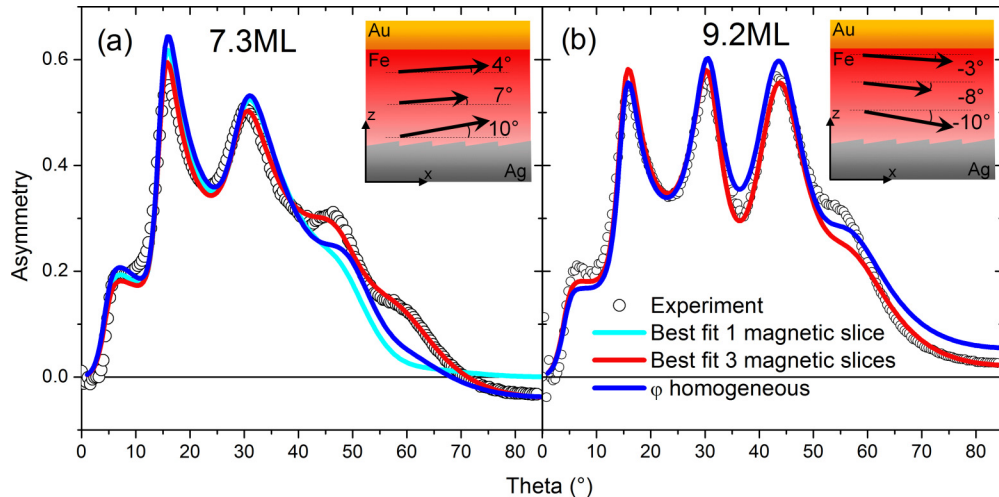


FIG. 5. (Color online) Magnetic asymmetries measured by SXRM (circles) in a remanent state at 20 K using circularly polarized light and photons energy of 706.6 eV for (a) 7.3- and (b) 9.2-ML-thick Fe layers. Solid lines correspond to best fits using different free-parameter sets and calculated curves (see text). Insets illustrate the model of the magnetic configuration used for the best fit.

than the fingerprint of the beam at the sample surface, or a canted magnetization configuration [43]. To separate out both configurations, we tried to reproduce the experiment by combining independently calculated asymmetries for pure oop and ip magnetization [Fig. 4(c)]. On the one hand, to fit the low-angle part, we are prompted to set the proportion of ip domain to about 65% with only 35% oop domain, which does not allow us to reproduce the large-angle part. On the other hand, increasing the proportion of oop domains to fit the large-angle area prevents us from fitting the low-angle part. We therefore conclude that the magnetization is in a canted state with a canting angle of 53°.

Figures 4(b) and 4(d) display the results for the 5-ML-thick sample. The shape of the asymmetries is similar, with a weaker signal at large angles. Considering only two parameters, a very good agreement is obtained for an average magnetic moment $m_{\text{Fe}} = 2.8\mu_B \pm 0.5\mu_B$ and an average tilt angle $\varphi = 6^\circ \pm 4^\circ$ under an applied field and $\varphi = 28^\circ \pm 3^\circ$ at remanence. Those angles are smaller with respect to 4.2 ML, indicating a smaller oop magnetic anisotropy for thicker Fe film, as expected for a SRT.

Figures 5(a) and 5(b) show asymmetries collected in a remanent state at 706.6 eV for 7.3 and 9.2 ML, respectively. Both asymmetries present a signal different from zero at large angles, revealing the presence of an oop component. Any attempt to fit those asymmetries assuming a uniform magnetization throughout the layer failed [light blue solid line in Fig. 5(a)]. As shown in [41], for Fe thicknesses superior to 5.5 ML, the spatial resolution of SXRM is in the 2–3-ML range in the vicinity of the Fe L_3 edge. Hence the Fe layer is divided into three slices of homogeneous magnetization, which leads to six free parameters: three magnetization amplitudes and three tilt angles φ . In order to reduce the number of free parameters, the three magnetization amplitudes are determined separately by analyzing the magnetic asymmetry collected by switching the magnetic field applied in the direction transverse to the scattering plane (along the y axis) and using linear π

polarization (transverse mode). Because of the specific geometrical dependence of the three magnetization orientations of the atomic scattering factor, this π - π acquisition geometry probes only the transverse component of magnetization [41] and allows us to separate out the amplitude of the magnetization from the value of the tilt angle. For 7.3 ML, the magnetic moments for the three slices are $2.9\mu_B \pm 0.2\mu_B/2.2\mu_B \pm 0.05\mu_B/2.7\mu_B \pm 0.2\mu_B$, from Ag to Au, in good agreement within the error bars of previous results [41]. Then the three tilt angles φ are derived by analyzing the asymmetry obtained in the longitudinal geometry [Fig. 5(a)]. The best fit is obtained for the noncollinear distribution $10^\circ/7^\circ/4^\circ$ from the Ag to the Au interface with a $\pm 5^\circ$ error bar, as sketched in Fig. 5(a). The same analysis is carried out for the 9.2-ML sample [Fig. 5(b)], leading to an enhancement of 20% to 30% of the magnetic moment at both interfaces with the following distribution of tilt angles: $-10^\circ/-8^\circ/-3^\circ (\pm 5^\circ)$ from Ag to Au. The dark blue solid lines in Figs. 5(a) and 5(b) display the calculations for a uniform tilt angle corresponding to the average value of the three tilt angles φ . This shows the strong improvement provided by the graded profile at large angles.

Finally, we present the result obtained in a remanent state for an Fe thickness of 5.9 ML (Fig. 6), corresponding to an intermediate thickness range. The amplitude of the asymmetry observed at large angles lies in between the values observed for the 5- and 7.3-ML-thick Fe films. We observe that at small angle, around 12°, the shape of the asymmetry for 5.9 ML is different than that of the asymmetries for other Fe thicknesses. This is ascribed to a slight modification of the structure since the 5.9-ML sample comes from another wedge with a thicker Au cover layer (mentioned previously). As the asymmetry is an interference term between charge- and magnetization-dependent scattering [40,44], a small change in the layer stacking will alter the shape of the asymmetry. Unlike for 4.2 and 5 ML, the refinement procedure, considering a unique magnetic layer corresponding to a constant magnetization profile and tilt angle, does not work. Considering three

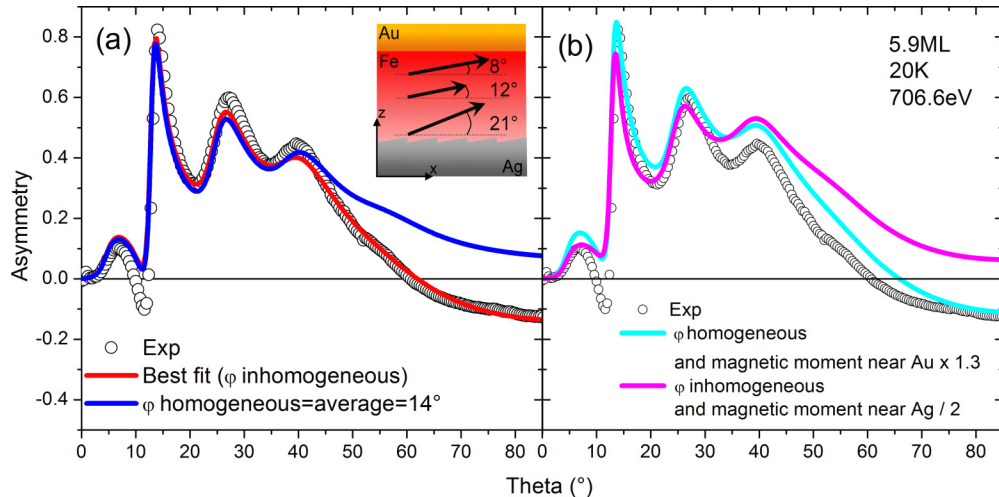


FIG. 6. (Color online) Magnetic asymmetry measured by SXRMR (circles) in a remanent state at 20 K using circularly polarized light at 706.6 eV for 5.9-ML-thick Fe layers. In (a) the red solid line represents the best fit with three magnetic slices with inhomogeneous magnetic amplitude and inhomogeneous titled angle φ . The model is sketched in the inset. The blue solid line represents the same model but with a homogeneous tilted angle $\varphi = 14^\circ$. In (b) the solid lines show theoretical asymmetry obtained for two different models (see text).

magnetic slices, with a 20%–30% increase in the magnetic moment near both Ag and Au interfaces, as found in [41], the best fit (red solid line) leads to the inhomogeneous canting profile $21^\circ/12^\circ/8^\circ \pm 5^\circ$ from the Ag to Au interfaces, as sketched in Fig. 6(a).

In order to illustrate the improvement with regard to a constant tilt angle across the layer, the dark blue solid line in Fig. 6(a) shows one calculation for a uniform tilt angle corresponding to the average value of the three tilt angles $\varphi = 14^\circ$. The strong disagreement with the experimental curve confirms the need for an inhomogeneous tilt angle. Furthermore, this calculation surprisingly reveals that a change in sign of the asymmetry is not necessarily related to a change in sign of the oop component. Figure 6(b) displays two additional calculations compared with the experimental data to show how variations in the inhomogeneity of the magnetic parameters can modify the asymmetry. First, starting from the same model as the one yielding the dark blue asymmetry in Fig. 6(a) (homogeneous φ), an increase in the magnetization amplitude of the top slice (near Au) by 30% provokes a change in sign of the asymmetry at large angles from positive to negative values [light blue curve in Fig. 6(b)]. Second, starting from the best model [red line in Fig. 6(a)] with variation of φ throughout the layer, a change in sign of the asymmetry at large angles can be caused by a reduction in the magnetization amplitude of the bottom slice by 50% [solid pink line in Fig. 6(b)]. Those different asymmetry curves representing different magnetic configurations show that changes in the values, either of the magnetization amplitude or of the tilt angle, at various locations across the layer affect the shape and the sign of the asymmetry at large angles. This emphasizes the importance of the benefit of using different configurations of acquisition to determine as unique a model as possible. In this study, the profile of the magnetization amplitude was independently resolved by using the transverse mode, and the profile of the tilt angles was determined with the longitudinal configuration.

With regard to the best model derived from our analysis of the asymmetry for the 5.9-ML sample, it is worth noting that the change between the tilt angle in the first layer and the other one is much larger than in the cases with 7.3 and 9.2 ML. It must be mentioned that the magnetization and thus the tilt angles are determined for slightly thinner slices (2 ML) than those for the 7.3-ML sample (2.5 ML). Therefore, one may wonder whether the result of such a large change could be due to the diminution of the vertical integration volume. As a test, we tried to fit the asymmetry of 7.3 ML with four magnetic slices, leading to magnetic slices 1.8 ML thick. The values of the tilt angles in the slice in contact with Ag did not increase. Hence we believe that for 5.9 ML, the larger value of the tilt angle for the first slice relative to the upper one is an indication that the perpendicular magnetic anisotropy at the interface remains strong enough to induce a larger tilt. However, the asymmetry is highly sensitive to the inhomogeneity of the magnetic parameters of each slice. Therefore we cannot rule out that the larger difference between the first and the other slices in the 5.9-ML sample compared to the 7.3- and 9.2-ML samples could be related to the uncertainties of the magnetization amplitude derived from the analysis of the transverse-mode acquisition.

In order to compare our results to independent macroscopic measurements of the tilt angle, Fig. 7 shows all average values of the tilt angle derived from the SXRMR spectra compared to the angles obtained from longitudinal MOKE. The good agreement between the data gives an indication of the robustness of the analysis. We would like to point out that the analysis of a 6.4-ML-thick sample yields the tilt angle profile $19^\circ/15^\circ/13^\circ$, and the average value $\varphi = 15.7^\circ$ reported in Fig. 7 is also in very good agreement with MOKE results. For 9.2 ML, the negative value found for the canting angle shows the sensitivity of SXRMR to the oscillating behavior induced by the presence of quantum well states in this Fe layer [22,32].

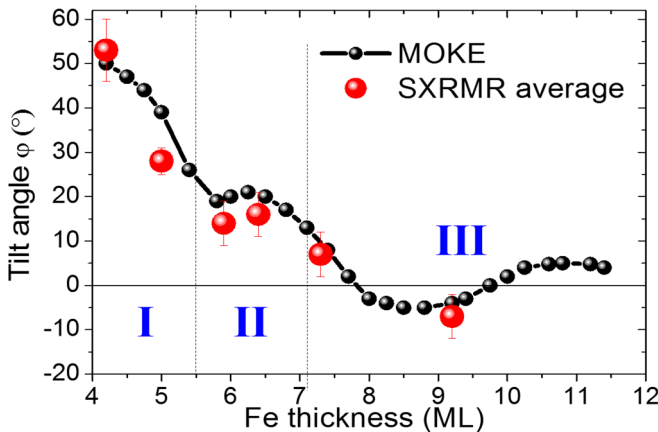


FIG. 7. (Color online) Comparison of tilt angles as a function of Fe thickness at 20 K for Au-covered samples at remanence from MOKE and SXRMR experiments. Above $t_{\text{Fe}} = 5.5 \text{ ML}$, the SXRMR data points correspond to the average of the tilted angles in the graded profile. Three different area are discussed in the text.

IV. DISCUSSION

These results have led us to identify three thickness areas: (I) $t_{\text{Fe}} < 5.5 \text{ ML}$, (II) $5.5 \text{ ML} < t_{\text{Fe}} < 7.3 \text{ ML}$, (III) $t_{\text{Fe}} > 7.3 \text{ ML}$ (Fig. 7). For all these Fe thicknesses, when the magnetization is forced to be along the steps, in the transverse direction, there is no oop magnetic contribution. In that case the magnetic vector lies in the terrace plane and in the surface plane. It is only when the magnetization rotates perpendicular to the steps that this magnetic vector is no longer parallel to the surface plane and an oop component appears. Indeed, the competition between the magnetocrystalline anisotropy and the shape anisotropy tilts the magnetization from the surface plane toward the terrace plane when the magnetization is oriented perpendicular to the step edges [22]. Below we first discuss results for area (I) and area (III) before looking at the more complex results for area (II).

In the first thickness area ($t_{\text{Fe}} < 5.5 \text{ ML}$), the canted magnetization is found to be uniform along the growth axis within the limit of our spatial resolution, which means we cannot exclude some inhomogeneity. The tilt angle is large in the remanent state and is strongly reduced under an applied magnetic field of 1600 Oe. At remanence, there is a competition between the shape anisotropy favoring an in-plane magnetization and the surface/interface perpendicular anisotropy, which leads to a canted configuration with a tilt angle changing rapidly with increasing thickness. This is the SRT regime.

For $t_{\text{Fe}} > 5.5 \text{ ML}$, the analysis reveals unambiguously the inhomogeneity of the canted magnetization profile, with the highest value of the tilt angle near the vicinal surface. The determination of the inhomogeneity is correlated to the proper analysis of the profile of the magnetic amplitude. Area (III) is characterized by an angle close to the Ag interface, very similar to the vicinal angle (13.3°) within error bars. The upper angular values approach zero when getting closer to the top interface. The observation of such a tilt angle close to the Ag stepped substrate indicates a competition between the magnetocrystalline anisotropy and the shape anisotropy.

For Fe grown on flat Ag, the shape anisotropy is dominant for thicknesses above 5 ML [45]. However, when Fe is grown on vicinal surface, the magnetocrystalline anisotropy is strong enough to overcome the shape anisotropy at the Ag interface. After the first 2–3 ML, either the inclination of the crystalline lattice is reduced or the shape anisotropy tends to align the magnetization within the sample plane.

Concerning area (II), the behavior of the tilt angle in the first two to three Fe MLs is higher than the inclination of the vicinal angle. This can be ascribed to the tail of the SRT, adding a term to the global anisotropy (PMA, shape, and magnetocrystalline) and therefore increasing the oop component. Whereas the oop component is related only to SRT for a thickness below 5.5 ML and is due only to the Ag steps for thicknesses above 7.3 ML, in between, there is a mix of both SRT and Ag step contributions.

While the origin of the canted magnetization is clear, the origin of the inhomogeneity, especially for layers thinner than the exchange length estimated to 3 nm for Fe [16,17,23], can be twofold. One possibility is that the inhomogeneity comes from a reduced inclination of the bcc Fe lattice when the thickness of the layer is increased. Another one is that atoms located at the steps play a specific role in inducing an inhomogeneity. Although embedded, they could be a source of perpendicular anisotropy. For uncovered atoms on a stepped surface, the effect is reduced when going from a one-dimensional structure (atom only along the edge) to a two-dimensional structure (atoms covering the terraces) [46], but the edge atoms can still contribute to a PMA enhancement [47,48]. Therefore the atoms at the edge could be at the origin of higher oop component close to the substrate. At this point, our analysis cannot distinguish whether the inhomogeneity comes from the depth-dependent modification of the magnetocrystalline anisotropy due to the less defined steps with increasing thickness or from the edge atoms, whose effect is reduced with a thicker layer.

The study of the dependence of the magnetization profile for different vicinal angle values should not help to differentiate proposed origins of the inhomogeneity. It is expected that larger terraces (smaller vicinal angle) will reduce the effect of the inclination as well as the effect of the atoms along the steps due to their reduced number and vice versa. In order to get more insight into that issue, we measured two asymmetries, before and after reversing the orientation of the terraces through a 180° azimuthal rotation of the sample (Fig. 8). The data are collected at a position along the wedge corresponding to 5 ML. The longitudinal applied field is flipped at each data point starting with the same initial orientation (black arrows in Fig. 8). For the two different terraces orientations, the experimental asymmetries (circles) in Fig. 8 show a change in sign at large angles and the same sign at low angles. To explain these results we can consider separately the effect of the terraces inclination (panel A of the sketch in Fig. 8) and the effect of the PMA of the step atoms (panel B of the sketch in Fig. 8). First, we consider the terrace inclination effect. The magnetocrystalline anisotropy coming from the terrace inclination contributes to a certain tilt value and hence to a certain oop contribution since the applied field is not strong enough to align all the magnetic moments in the surface plane. As the initial direction of the applied field is the same

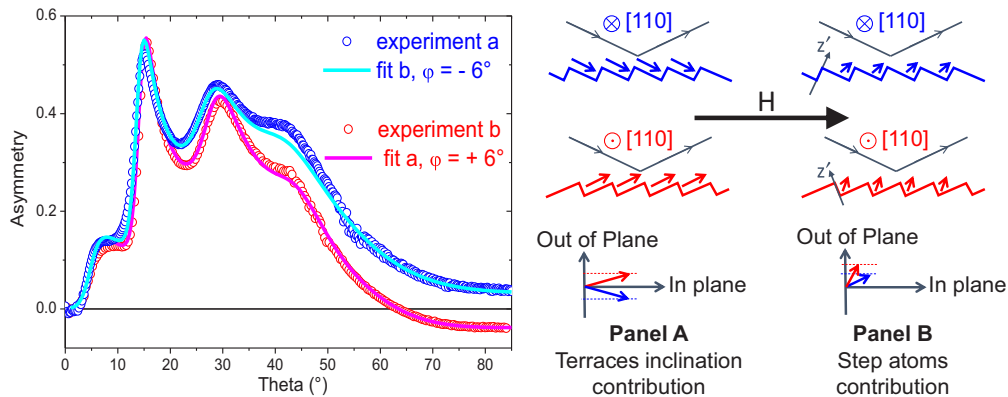


FIG. 8. (Color online) Experimental asymmetries for 5 ML (circles) and best fit (lines) obtained at 706.6 eV with circular polarization by reversing a longitudinally applied magnetic field of $H = 1600$ Oe (black arrow). The difference between blue and red curves is the orientations of the steps, as shown in the top and middle sketches. The sketches show two different oop contributions: one coming from the terraces inclination and one coming from the step atoms.

when the sample is rotated, there is a change in sign of the oop contribution, whereas the ip contribution is not modified (panel A of the sketch in Fig. 8). Second, we consider the PMA of the step atoms as the main origin of the tilt of the average magnetization. In a schematic view, at remanence, the magnetization is perpendicular to the terraces, i.e., tilted by $+13.3^\circ$ from the normal to the sample surface, as displayed by the z' axis in panel B of Fig. 8. However, due to the surrounding atoms and to the applied field, the magnetization of these step atoms is probably tilted in the direction of the applied field, contributing to a certain oop component [47]. After the rotation of the sample under zero external field, the magnetization of the step atoms is probably rotated and tilted by -13.3° (along the tilted z' axis) but still pointing towards the surface due to the PMA. Assuming the PMA plays a role, the magnetization is not reversed when the magnetic field is turned on and is likely to be just tilted in the direction of the applied field, leading to an unreversed and possibly different oop component (panel B of the sketch in Fig. 8). This is in direct contrast to the experimental result. Indeed, it turns out that the amplitude of the asymmetry at large angles is opposite with a similar amplitude, and the fit of both asymmetries leads to the same angular absolute value of 6° within $\pm 0.2^\circ$. This result suggests the change in the asymmetry's sign is dominantly related to the magnetocrystalline anisotropy coming from the terrace inclination. Therefore the gradient of the canting angle is likely to depend on the modification of that magnetocrystalline anisotropy with a thicker sample.

Finally, although theoretically discussed [19], the depth dependence of the magnetization in the limit of a small number of monolayers remains elusive since no quantitative

determination has been proposed up to now. We did not find calculations predicting modifications of the canting angle along the growth axis at the subnanometer scale. However, in the theoretical approaches we point out that (i) the films are often considered with a symmetric interface, while our study concerns strongly different interfaces, and (ii) when dedicated to canting magnetization in thin films, most of the parameters (magnetic amplitude, magnetic stiffness) are generally considered to be constant across the film [8], which is not necessarily correct.

V. CONCLUSION

In conclusion, this work has revealed the inhomogeneity of the perpendicular canting magnetization for a layer as thin as 0.85 nm (5.9 ML). The amplitude of the tilt angle is quantitatively determined by SXRMR as well as its variation with increasing distance from the interface. The inhomogeneity has been ascribed to the modification of the balance of various anisotropies across the layer thickness. This work opens the way to probe fine details of interfacial magnetization modifications induced by external excitations like current and electric field.

ACKNOWLEDGMENTS

We are grateful to H. Popescu and R. Gaudemer for smoothly running the SEXTANTS beamline. Technical support from H. Menge and W. Greie at the Max-Planck-Institut für Mikrostrukturphysik and S. Garaudée at the Institut Néel are acknowledged.

-
- [1] A. D. Kent, *Nat. Mater.* **9**, 699 (2010).
 - [2] D. Suess, J. Lee, J. Fidler, and T. Schrefl, *J. Magn. Magn. Mater.* **321**, 545 (2009).
 - [3] Y. Y. Zou, J. P. Wang, C. H. Hee, and T. C. Chong, *Appl. Phys. Lett.* **82**, 2473 (2003).
 - [4] M. Albrecht, G. Hu, I. L. Guhr, T. C. Ulbrich, J. Boneberg, P. Leiderer, and G. Schatz, *Nat. Mater.* **4**, 203 (2005).
 - [5] R. Sbiaa, R. Law, E.-L. Tan, and T. Liew, *J. Appl. Phys.* **105**, 013910 (2009).
 - [6] U. Roy, H. Seinige, F. Ferdousi, J. Mantey, M. Tsoi, and S. K. Banerjee, *J. Appl. Phys.* **111**, 07C913 (2012).
 - [7] Y. Zhou, J. Persson, S. Bonetti, and J. Åkerman, *Appl. Phys. Lett.* **92**, 092505 (2008).

- [8] T. N. A. Nguyen, Y. Fang, V. Fallahi, N. Benatmane, S. M. Mohseni, R. K. Dumas, and J. Åkerman, *Appl. Phys. Lett.* **98**, 172502 (2011).
- [9] S. M. Watson, T. Hauet, J. A. Borchers, S. Mangin, and E. E. Fullerton, *Appl. Phys. Lett.* **92**, 202507 (2008).
- [10] F. Yildiz, M. Przybylski, and J. Kirschner, *Phys. Rev. Lett.* **103**, 147203 (2009).
- [11] J. Choi, B.-C. Min, J.-Y. Kim, B.-G. Park, J. H. Park, Y. S. Lee, and K.-H. Shin, *Appl. Phys. Lett.* **99**, 102503 (2011).
- [12] J. de la Venta, M. Erekhinsky, S. Wang, K. G. West, R. Morales, and I. K. Schuller, *Phys. Rev. B* **85**, 134447 (2012).
- [13] Y. Shiratsuchi, H. Noutomi, H. Oikawa, T. Nakamura, M. Suzuki, T. Fujita, K. Arakawa, Y. Takechi, H. Mori, T. Kinoshita, M. Yamamoto, and R. Nakatani, *Phys. Rev. Lett.* **109**, 077202 (2012).
- [14] Y. Y. Wang, C. Song, B. Cui, G. Y. Wang, F. Zeng, and F. Pan, *Phys. Rev. Lett.* **109**, 137201 (2012).
- [15] D. L. Mills, *Phys. Rev. B* **39**, 12306 (1989).
- [16] R. C. O'Handley and J. P. Woods, *Phys. Rev. B* **42**, 6568 (1990).
- [17] H. N. Bertram and D. I. Paul, *J. Appl. Phys.* **82**, 2439 (1997).
- [18] A. P. Popov, A. V. Anisimov, O. Eriksson, and N. V. Skorodumova, *Phys. Rev. B* **81**, 054440 (2010).
- [19] P. Jensen and K. Bennemann, *Surf. Sci. Rep.* **61**, 129 (2006).
- [20] N. de Sousa, A. Apolinario, F. Vernay, P. M. S. Monteiro, F. Albertini, F. Casoli, H. Kachkachi, and D. S. Schmool, *Phys. Rev. B* **82**, 104433 (2010).
- [21] Y. Z. Wu, C. Won, H. W. Zhao, and Z. Q. Qiu, *Phys. Rev. B* **67**, 094409 (2003).
- [22] J. Li, M. Przybylski, Y. He, and Y. Z. Wu, *Phys. Rev. B* **82**, 214406 (2010).
- [23] B. Laenens, N. Planckaert, J. Demeter, M. Trekels, C. L'abbé, C. Strohm, R. Rüffer, K. Temst, A. Vantomme, and J. Meersschaut, *Phys. Rev. B* **82**, 104421 (2010).
- [24] T. Kawauchi, K. Fukutani, M. Matsumoto, K. Oda, T. Okano, X. W. Zhang, S. Kishimoto, and Y. Yoda, *Phys. Rev. B* **84**, 020415 (2011).
- [25] H.-C. Hou, B. J. Kirby, K. Z. Gao, and C.-H. Lai, *Appl. Phys. Lett.* **102**, 162408 (2013).
- [26] B. J. Kirby, J. E. Davies, K. Liu, S. M. Watson, G. T. Zimanyi, R. D. Shull, P. A. Kienzle, and J. A. Borchers, *Phys. Rev. B* **81**, 100405 (2010).
- [27] J.-M. Tonnerre, M. Przybylski, M. Ragheb, F. Yildiz, H. C. N. Tolentino, L. Ortega, and J. Kirschner, *Phys. Rev. B* **84**, 100407 (2011).
- [28] M. Elsen, J. H. Gao, V. Repain, C. Chacon, Y. Girard, J. Lagoute, G. Rodary, J. Ferré, and S. Rousset, *Europhys. Lett.* **88**, 27006 (2009).
- [29] R. K. Kawakami, E. J. Escoria-Aparicio, and Z. Q. Qiu, *Phys. Rev. Lett.* **77**, 2570 (1996).
- [30] U. Bauer and M. Przybylski, *Phys. Rev. B* **81**, 134428 (2010).
- [31] U. Bauer, M. Dabrowski, M. Przybylski, and J. Kirschner, *J. Magn. Magn. Mater.* **323**, 1501 (2011).
- [32] J. Li, M. Przybylski, F. Yildiz, X. D. Ma, and Y. Z. Wu, *Phys. Rev. Lett.* **102**, 207206 (2009).
- [33] M. Dabrowski, T. R. F. Peixoto, M. Pazgan, A. Winkelmann, M. Cinal, T. Nakagawa, Y. Takagi, T. Yokoyama, F. Bisio, U. Bauer, F. Yildiz, M. Przybylski, and J. Kirschner, *Phys. Rev. Lett.* **113**, 067203 (2014).
- [34] N. Jaouen, J.-M. Tonnerre, G. Kapoujian, P. Taunier, J.-P. Roux, D. Raoux, and F. Sirotti, *J. Synchrotron Radiat.* **11**, 353 (2004).
- [35] M. Sacchi, N. Jaouen, H. Popescu, R. Gaudemer, J. M. Tonnerre, S. G. Chiuzbaian, C. F. Hague, A. Delmotte, J. M. Dubuisson, G. Cauchon, B. Lagarde, and F. Polack, *J. Phys. Conf. Ser.* **425**, 072018 (2013).
- [36] J. B. Kortright and S.-K. Kim, *Phys. Rev. B* **62**, 12216 (2000).
- [37] D. Haskel, E. Kravtsov, Y. Choi, J. Lang, Z. Islam, G. Srager, J. Jiang, S. Bader, and P. Canfield, *Eur. Phys. J. Spec. Top.* **208**, 141 (2012).
- [38] J.-M. Tonnerre, E. Jal, E. Bontempi, N. Jaouen, M. Elzo, S. Grenier, H. L. Meyerheim, and M. Przybylski, *Eur. Phys. J. Spec. Top.* **208**, 177 (2012).
- [39] S. Macke and E. Goering, *J. Phys. Condens. Matter* **26**, 363201 (2014).
- [40] J. M. Tonnerre, L. Sèvre, D. Raoux, G. Soulié, B. Rodmacq, and P. Wolfers, *Phys. Rev. Lett.* **75**, 740 (1995).
- [41] E. Jal, M. Dabrowski, J.-M. Tonnerre, M. Przybylski, S. Grenier, N. Jaouen, and J. Kirschner, *Phys. Rev. B* **87**, 224418 (2013).
- [42] J. P. Hannon, G. T. Trammell, M. Blume, and D. Gibbs, *Phys. Rev. Lett.* **61**, 1245 (1988).
- [43] H. Tang, D. Weller, T. G. Walker, J. C. Scott, C. Chappert, H. Hopster, A. W. Pang, D. S. Dessau, and D. P. Pappas, *Phys. Rev. Lett.* **71**, 444 (1993).
- [44] F. de Bergevin, M. Brunel, R. M. Galéra, C. Vettier, E. Elkaïm, M. Bessière, and S. Lefèuvre, *Phys. Rev. B* **46**, 10772 (1992).
- [45] N. C. Koon, B. T. Jonker, F. A. Volkening, J. J. Krebs, and G. A. Prinz, *Phys. Rev. Lett.* **59**, 2463 (1987).
- [46] P. Gambardella, A. Dallmeyer, K. Maiti, M. C. Malagoli, W. Eberhardt, K. Kern, and C. Carbone, *Nature (London)* **416**, 301 (2002).
- [47] S. Rusponi, T. Cren, N. Weiss, M. Epple, P. Buluscheck, L. Claude, and H. Brune, *Nat. Mater.* **2**, 546 (2003).
- [48] J. Geshev, A. Gündel, I. Zaharieva, and J. E. Schmidt, *Appl. Phys. Lett.* **101**, 132407 (2012).